(Preprint) AAS 22-594

APPLICATION OF TISSERAND'S CRITERION AND THE LIDOV-KOZAI EFFECT TO STORM'S TRAJECTORY DESIGN

Michael A. Shoemaker*, David C. Folta†, and David G. Sibeck‡

The Solar-Terrestrial Observer for the Response of the Magnetosphere (STORM) concept recently completed its Phase A design funded by NASA's Heliophysics Medium-class Explorers program. The mission design required a lunar gravity assist to insert the single spacecraft into a 30-Earth-radii circular geocentric science orbit inclined 90 degrees to the ecliptic. STORM's trajectory design leveraged several interesting gravitational effects from third bodies. This paper describes our application of Tisserand's criterion for finding feasible transfers and lunar gravity assist trajectories, and the Lidov-Kozai effect to design a maneuver-free science orbit optimization and decommissioning strategy.

INTRODUCTION

Spacecraft operating in cislunar space are subject to gravitational effects from the Earth, Moon and Sun that can create important considerations for mission designers. Tisserand's criterion is an approximation within the circular restricted three-body problem (CR3BP), where a satellite performing a flyby of the secondary will have a nearly constant parameter that relates the pre-flyby and post-flyby semimajor axis, eccentricity, and ecliptic inclination with respect to the primary. The Lidov-Kozai effect (LKE) is a dynamic coupling between eccentricity and inclination for satellites in high-ecliptic-inclination orbits under the effect of luni-solar gravitational perturbations, leading to a secular growth in eccentricity. These two effects were applied to the mission design for the Solar-Terrestrial Observer for the Response of the Magnetosphere (STORM), which recently completed its Phase A design at NASA Goddard Space Flight Center (GSFC) funded by NASA's Heliophysics Medium-class Explorers (MIDEX) program. This paper describes STORM's unique orbit design, which leveraged knowledge of Tisserand's criterion and the LKE. Sharing this orbit design experience may aid future mission planners who wish to utilize similar orbits in cislunar space.

STORM MISSION OVERVIEW

The STORM mission's overall science objective was to quantify the fundamental processes involved in the end-to-end circulation of energy throughout the global solar wind-magnetosphere-ionosphere system. To achieve this mission, the spacecraft's science orbit consisted of a 30-Earth-radii (R_E) circular obit inclined approximately 90 degrees to the solar ecliptic. This science orbit

*Aerospace Engineer, Navigation and Mission Design Branch (Code 595), NASA Goddard Space Flight Center, Greenbelt, MD, 20771, USA.
†Aerospace Engineer, Navigation and Mission Design Branch (Code 595), NASA Goddard Space Flight Center, Greenbelt, MD, 20771, USA.
‡STORM Principal Investigator, Heliophysics Science Division (Code 670), NASA Goddard Space Flight Center, Greenbelt, MD, 20771, USA.

provided a view of the subsolar magnetopause, auroral oval, and ring current from multiple vantage points, covering the full range of latitudes and local times, as well as in-situ sampling of the interplanetary magnetic field and solar wind plasma. Figure 1 illustrates the science orbit, with annotations for these targets and their significance to the science questions intended to be answered by the mission. The geometry of the science orbit, which has a period of approximately 9.65 days, allowed for a nearly continuous viewing of the magnetopause, and long duration views of the north and south polar auroral regions. Additional details about STORM's science can be found on the mission website*, as well as in references related to a precursor cubesat mission[1] and a future lunar payload with a soft X-ray imager instrument similar to STORM's.[2]

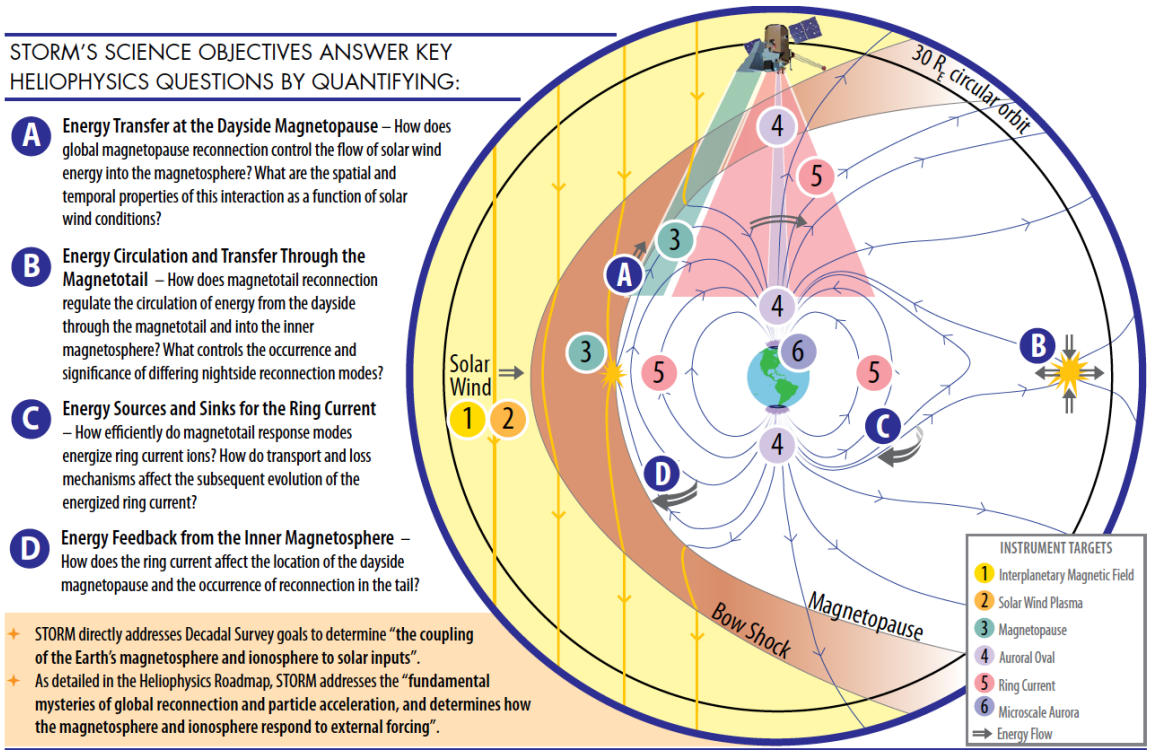

Figure 1. Illustration of STORM's 30-R_E circular science orbit with major science questions to be answered by the mission.

STORM had a Launch Readiness Date (LRD) of 1 July 2026. Figure 2 shows an illustration of the launch, transfer, and final science orbit, along with major events in the mission timeline, for the design reference mission (DRM) with a launch epoch on 3 July 2026. STORM was planned to be initially launched into a highly eccentric orbit, taking it past the orbit of the Moon, to a maximum distance of approximately 100 to 157 R_E, depending on launch epoch. After achieving apogee and returning back towards the Moon, the spacecraft would perform a lunar gravity assist (LGA) to change its ecliptic inclination into the required near 90-deg value and to achieve a perigee of 30 R_E. After traveling for approximately 4 days post-LGA, the spacecraft would then perform its Science Orbit Insertion (SOI) maneuver near the 30 R_E perigee radius and circularize. Also denoted in Figure 2 are several Trajectory Correction Maneuvers (TCMs) used to clean up launch vehicle

*https://stormmission.com/

dispersions and other navigation and maneuver execution errors. Not shown in Figure 2 is TCM-4, which is performed a few days after SOI and is used predominately to clean up the desired science orbit after SOI maneuver execution errors.

The LGA was an enabling factor for this mission concept, as the ΔV required to directly insert into the science orbit would have been prohibitive for this Heliophysics MIDEX category of mission, given the mass and launch vehicle constraints. Of course, LGAs have previously been examined by others for inclination changes on Earth-orbiting satellites. The use of LGAs to insert into geosynchronous Earth orbit (GEO) has received much attention in the literature, for example, Refs. 3–6 and citations therein. This interest in geosynchronous orbit is unsurprising, given the large number of operational GEO satellites. The use of LGAs to insert into high-inclination orbits has received less attention than their use at GEO. Betts[7] discusses several optimal techniques, including using a LGA to insert into 24-hour Earth polar orbits, in addition to other types of orbit destinations. Lee et al.[8] describe single and double lunar swingby methods to insert into a 3×20 R_E, 90-deg equatorially inclined polar orbit for a past solar terrestrial physics mission proposal. One contribution of the present paper is a discussion of how Tisserand's criterion was used to inform our search for feasible transfer trajectories, and enable solutions to be found for each day in the lunar orbital period.

STORM's mission requirements included the following that are important for trajectory design:

- Science orbit ecliptic inclination $= 90 \pm 10$ deg.
- Science orbit radius $= 30 \pm 1$ R_E.
- Science orbit operational lifetime $= 2$ years.
- Spacecraft end-of-mission disposal lifetime $= 25$ years.

The remainder of this paper focuses on how Tisserand's criterion and the LKE were leveraged to enable the design for this mission concept. We also present a detailed Monte Carlo analysis of the science orbit stability and end-of-mission disposal, which are both affected by the 3rd-body perturbations underlying the LKE.

USING TISSERAND'S CRITERION FOR TRANSFER DESIGN

The Tisserand criterion is named after Félix Tisserand,[9] who discovered this approximation of the Jacobi constant while observing comet encounters with Jupiter.[10] The unitless Tisserand parameter T of a satellite is defined in the CR3BP as

$$T = \frac{1}{2a} + \sqrt{a(1-e^2)}\cos i \tag{1}$$

where a is the semimajor axis (normalized by the Earth-Moon distance), e is the eccentricity, and i is the ecliptic inclination (i.e. relative to the CR3BP's xy plane). For the purpose of analyzing T for the STORM mission, we treat the Sun and Moon motion as both being constrained to the ecliptic. A satellite's value of T is approximately constant in the CR3BP when computed before and after the flyby of the secondary, and is more accurate the further from the secondary it is computed. Likewise, Eq. 1 can be computed in an ephemeris model using the oscullating values for a, e, and i, recognizing that T is only approximately constant. Figure 3 is a plot of T that is computed using the oscullating elements from a representative STORM trajectory solution in an ephemeris model,

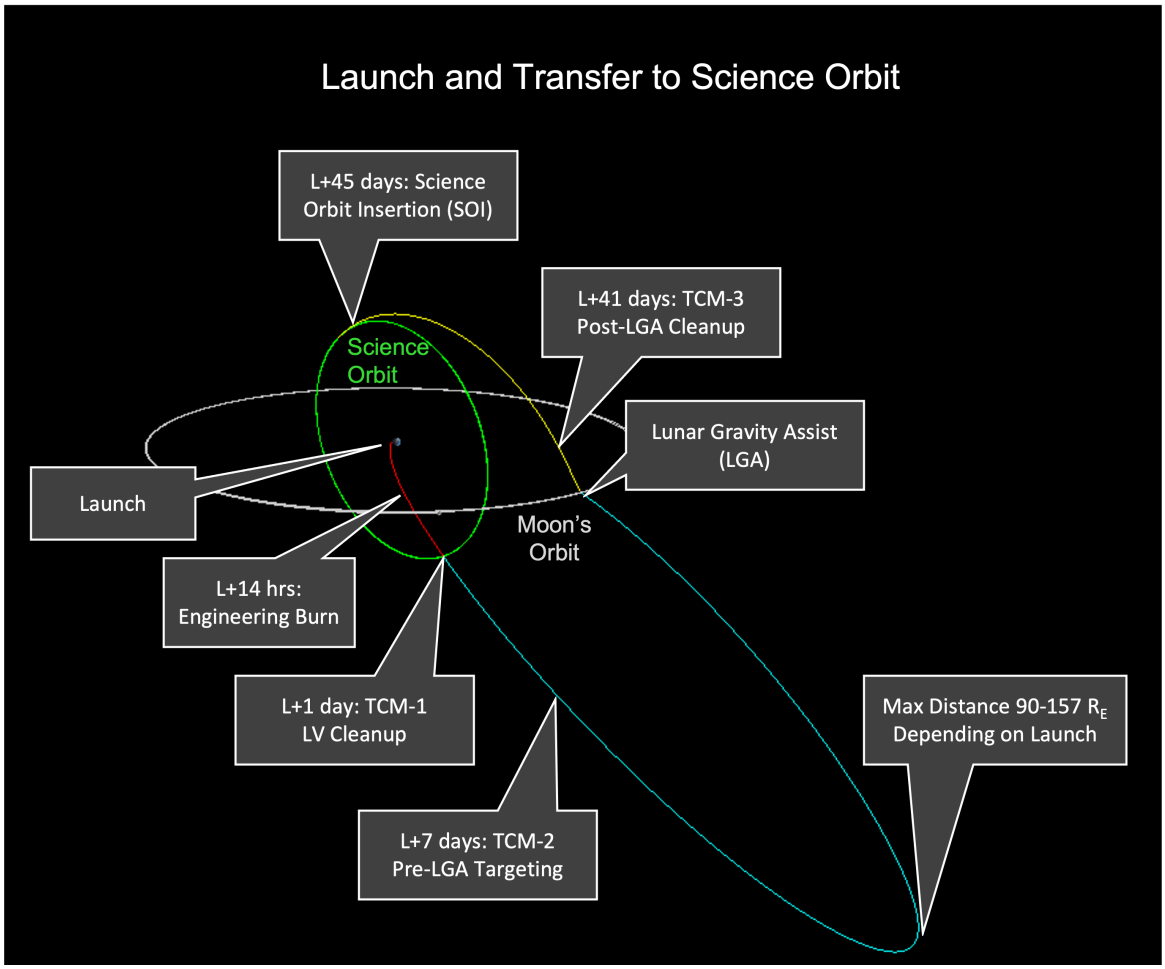

Figure 2. Illustration of STORM's design reference mission trajectory showing launch, transfer, and 30-R_E circular science orbit.

where the large dip at 22 days (in this case) is due to a violation in the underlying approximations used in the formulation of T as the spacecraft approaches the vicinity of the Moon. From Fig. 3 it is apparent that T is not perfectly constant, but still has the potential to serve as a useful reference value for mission design purposes as we describe below. The trajectory used in Fig. 3 represents one point solution from STORM's pre-Phase A design, and we will use a value of $T_{\text{ref}} = 0.66$ (which approximates the mean value in the plot) as the reference Jacobi constant value for the remainder of our design process described below.

The Tisserand criterion has been used by others in the past in various ways to support mission design. A Tisserand graph is one tool used to analyze feasible gravity assist sequences in interplanetary mission design,[11,12] which plots contours of spacecraft period and perihelion (*i.e.*, an alternative form of the Tisserand parameter). Reference 13 describes another graphical tool, the Tisserand-Poincaré graph, to design endgame strategies for ballistic captures at multibody systems like Jupiter and Saturn.

STORM's trajectory design used the Tisserand parameter to facilitate the identification of transfer

trajectories on each day in a lunar orbital period, to ensure that the mission could have maximum launch opportunities regardless of the position of the Moon on a given launch day. The conceptual significance of the Tisserand criterion for STORM can be better understood by viewing Figure 2. The size and shape of the yellow trajectory segment represents the post-LGA trajectory, which is not allowed to vary greatly, since its end points are constrained by the desired science orbit and the size of the Moon's orbit. But, the pre-LGA trajectory (the cyan trajectory segment) has more design flexibility, in terms of finding launch geometries and transfer times that intercept the Moon's B-plane conditions. Thus, the Tisserand criterion gives a theoretical basis for restricting our search for pre-LGA trajectories that yield a desired post-LGA trajectory. Because T is only an approximation in the CR3BP, we ultimately need solutions that work in an ephemeris model, which is why we use T as a method of restricting a grid search of initial conditions to our differential corrector. A nested differential corrector, as outlined in Figure 4, was developed to find trajectory solutions. For a given run of the targeter, an initial guess was required for the Transfer Trajectory Insertion (TTI) maneuver ΔV (denoted by ΔV_{TTI}), as well as the launch epoch (t_{launch}) and launch vehicle upper stage coast time between burnout and TTI (denoted by $\Delta t_{\mathrm{coast}}$). The reference value of T_{ref} was used to restrict the range of initial guesses on ΔV_{TTI} , since this maneuver determines the size of the trajectory leg from TTI to LGA.

The goal of the following procedure is to obtain an initial guess of ΔV_{TTI}. First, we solve for the semimajor axis a for the post-TTI trajectory, given the assumed constant reference value of $T_{\mathrm{ref}} = 0.66$. We can rewrite Eq. 1 as

$$0 = \frac{1}{2a} + \sqrt{a(1-e^2)}\cos i - T_{\mathrm{ref}} \tag{2}$$

As an approximation, let us replace e in Eq. 2 with the two-body relation $e = 1 - r_p/a$, where r_p is radius of perigee. Even though the trajectory from TTI to LGA will deviate from a two-body motion, the goal is to obtain an initial guess of ΔV_{TTI} that will feed into a full-force model differential corrector. The value r_p is known from the coast orbit parameters prior to TTI. The ecliptic inclination i is known from the coast orbit geometry at t_{TTI} (since the TTI maneuver does

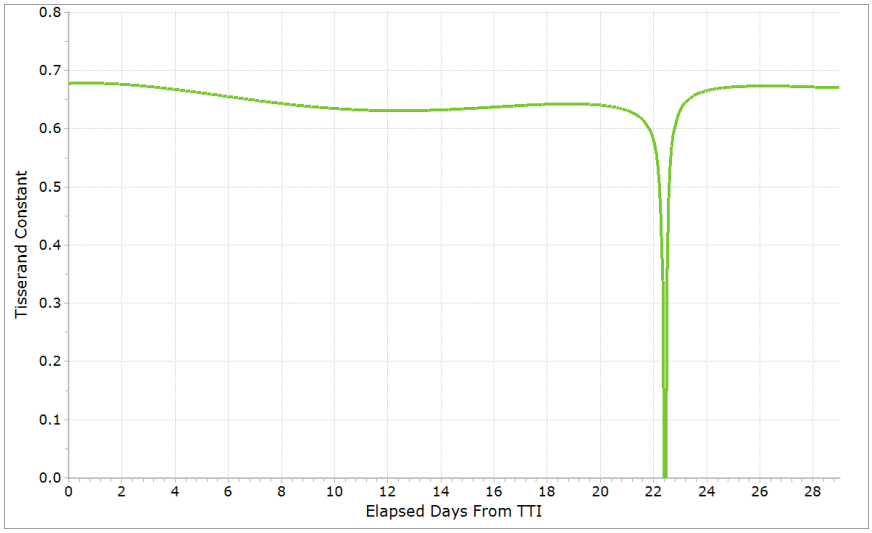

Figure 3. Computed Tisserand constant T for a representative STORM trajectory.

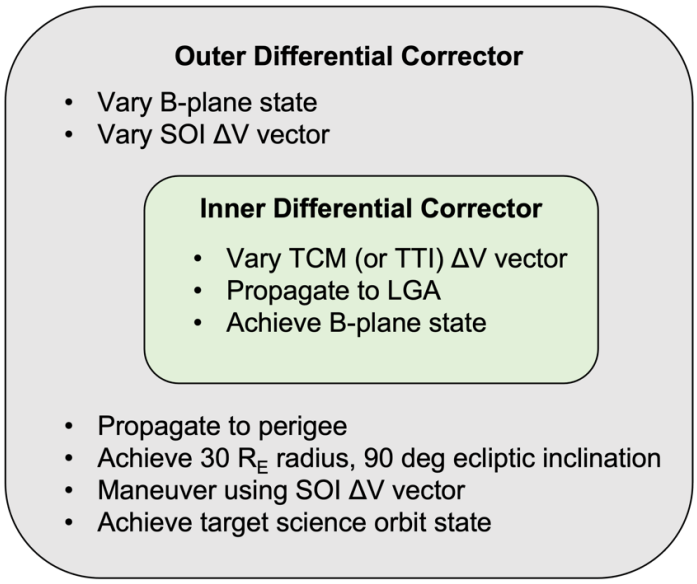

Figure 4. Overview of the nested differential corrector used to target STORMs transfer trajectory and science orbit.

not change the inclination). Thus, if the ecliptic inclination i, radius of perigee r_p, and T_{ref} are all known, then the remaining unknown value of a in Eq. 2 can be solved using a Newton-Rhapson root-finding method with an initial guess a_0. We denote this root as a^+_{TTI}, because it is the semi-major axis of the TTI-to-LGA leg immediately after TTI. Because the root finding is not sensitive to a_0, we use a constant value of $a_0 = 3.9 \times 10^5$ km, which comes from the same point solution that informed the definition of T_{ref}. Using the *vis-viva* equation, the newly found post-TTI velocity is

$$v^+_{\text{TTI}} = \sqrt{2\mu/r - \mu/a^+_{\text{TTI}}} \tag{3}$$

and the magnitude of the TTI maneuver is $\Delta V_{\text{TTI}} = v^+_{\text{TTI}} - v^-_{\text{TTI}}$.

The procedure in the grid search is as follows:

1. Loop over the search grid of t_{launch}, Δt_{coast}, and Δa.
2. Given the launch site geometry at t_{launch}, model the launch vehicle state at t_{burnout}, and propagate over Δt_{coast}, bringing the state to t_{TTI}.
3. Given the current pre-TTI conditions for r_p and i, solve Eq. 2 using Newton-Rhapson to obtain a^+_{TTI}.
4. Adjust a^+_{TTI} using the current grid search value: $a^+_{\text{TTI}} = a^+_{\text{TTI}} + \Delta a$.
5. Solve for v^+_{TTI} using Eq 3, which yields ΔV_{TTI} as the input initial guess to the differential corrector.
6. Run the nested differential correctors in Fig. 4 until all target states are achieved or the maximum number of iterations is exceeded.

The benefit of performing the grid search over Δa as opposed to ΔV_{TTI} itself is that we are guaranteed to remain in an elliptic orbit (in the two-body approximation) with a semimajor axis given by $a^{+}_{\mathrm{TTI}} + \Delta a$. It was found that when attempting to search over ΔV_{TTI} directly, it was sometimes possible to inadvertently place the spacecraft on a hyperbolic trajectory that escaped Earth, since the required TTI-to-LGA trajectory leg tended to have high eccentricities around 0.98.

TRANSFER DESIGN RESULTS

This section describes the results of running the Tisserand-based grid search described in the previous section. The Phase A design study examined launch sites at both Kennedy Space Center (KSC) in Florida and Wallops Flight Facility in Virginia, as these were among the available launch vehicle provider options in the Heliophysics MIDEX announcement of opportunity. As there were no significant differences in the resulting orbit profiles or ΔV usage, we only focus on the KSC results in the present paper.

A variety of commercial astrodynamics software was used for the STORM mission design. Systems Tool Kit and its Astrogator capability were used in pre-Phase A mission design, and FreeFlyer was used in Phase A design work. For the work described in this paper, the orbit is propagated in FreeFlyer version 7.6 with a Runge-Kutta 7-8 numerical integrator, with a variable step size and relative error tolerance of 1e-15. The dynamics model assumes Earth gravity (EGM96 10x10), Sun, Moon, and planetary point mass (DE430 ephemeris), cannonball solar radiation pressure, and cannonball atmospheric drag with an analytical density model (when drag was a concern in the reentry phases).

The grid search was run separately on each day starting on the LRD, with the goal of finding at least one valid trajectory solution per day, taking the spacecraft from launch until SOI and solving for the two deterministic maneuvers (ΔV_{TTI} and ΔV_{SOI}). The search grid $t_{\mathrm{launch}} \times \Delta a \times \Delta t_{\mathrm{coast}}$ typically had the following lengths: $10 \times 40 \times 10$ per day, but sometimes more stubborn days required a higher subdivision on the launch epoch by a factor of ten. The search over a month-long span after the LRD took approximately 3 days to run on a typical engineering notebook computer (MacBook Pro, 2.6 GHz 6-Core Intel i7, 16 GB RAM).

We ran the search over a total of 48 days beginning from the LRD, with the resulting transfer orbits plotted in Fig. 5, and some of the orbit characteristics plotted in Fig. 6. Figures 5 and 6 show that in general, there were two families of solutions, distinguished by the launch geometry, *i.e.*, reflected in $\Delta t_{\mathrm{coast}}$ (Fig. 6-a) and inertial longitude at launch (Fig. 6-c), as well as whether the TTI-to-LGA leg occurs mostly above or below the ecliptic plane. The majority of solutions are those having a short $\Delta t_{\mathrm{coast}}$ (between 10 and 20 minutes) and with a TTI-to-LGA leg below the ecliptic. A smaller set of solutions have a longer $\Delta t_{\mathrm{coast}}$ (between 40 to 50 minutes) and a resulting TTI-to-LGA leg above the ecliptic. Figures 6-b and -d show that all solutions have TTI-to-LGA durations under 40 days (which enables time for spacecraft checkout, navigation, and TCM planning prior to LGA), with a maximum distance of 157 $\mathrm{R_E}$ (consistent with the spacecraft's communications system design constraints). Note that STORM's science requirements did not constrain the science orbit beta angle β at the time of SOI; the variation in achieved β at t_{SOI} shown in Fig. 6-f is acceptable, and reflects the flexibility of the science orbit which allows such a wide number of LGA transfers to be found. It should also be noted that the differential corrector parameters for the B-plane targeting generally restricted the LGA to occur at the leading edge of the Moon's orbital motion, to enforce the LGA occuring on the return leg of the transfer and resulting in a LGA-to-SOI leg that traveled above the ecliptic. It is possible to find solutions at some epochs that have the LGA on the outbound

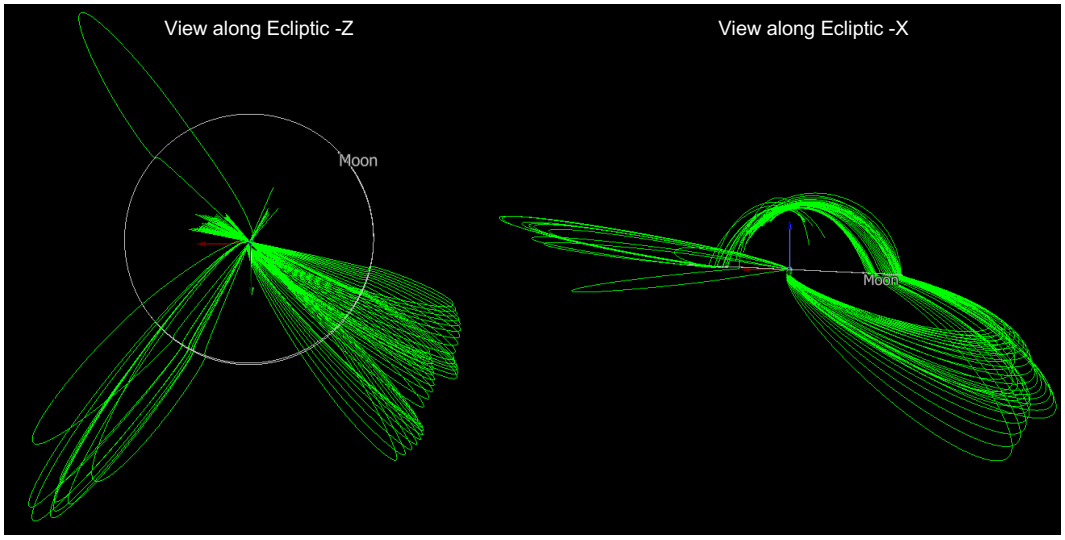

Figure 5. Top and side views of the resulting transfer orbit solutions (plotted from TTI to SOI in the inertial frame) for 48 days of launch opportunities.

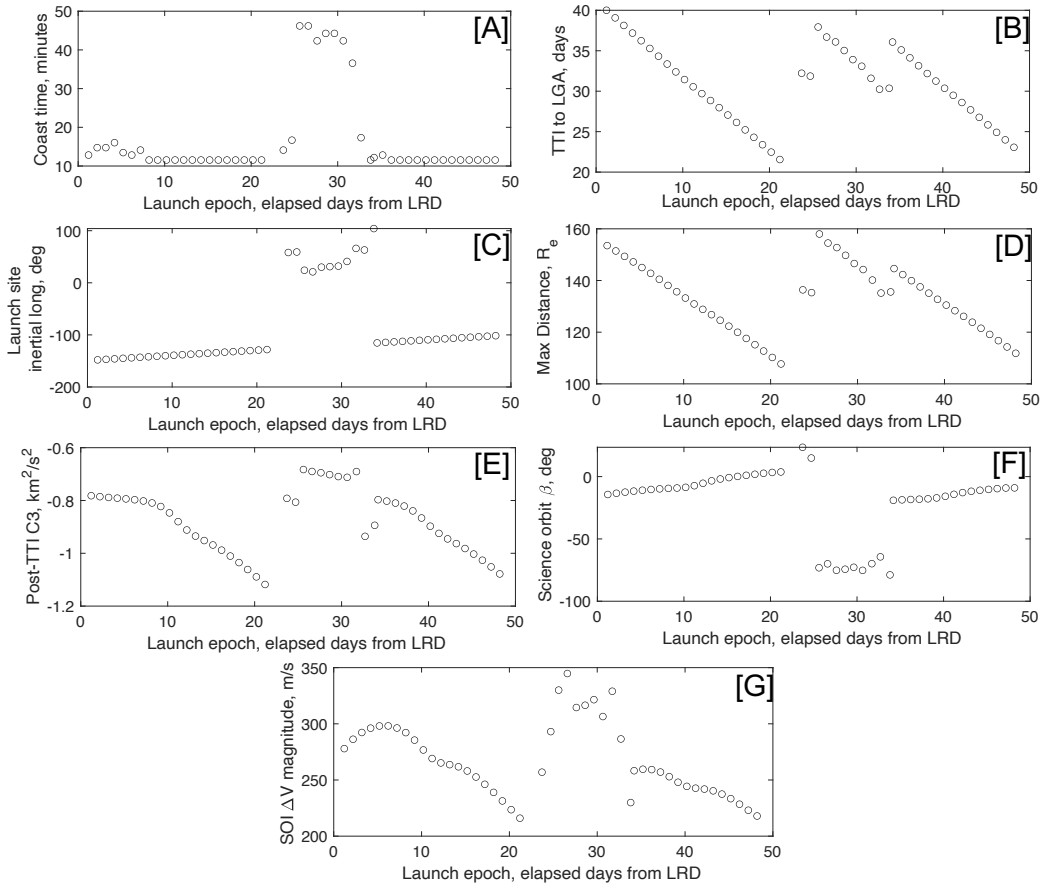

Figure 6. Plots showing properties of the transfer orbit solutions for 48 days of launch opportunities.

leg, as well as those that travel below the ecliptic during LGA-to-SOI, but we chose to constrain our solutions to the ones shown, to enable consistency in the mission design across launch epochs.

Figure 6-e shows the post-TTI C_3 from the launch vehicle upper stage vs. the solution on each launch epoch. Given the spacecraft mass, all required transfer orbit solutions were within the lift capabilities of the least-capable launch vehicle option provided. The ΔV_{SOI} also varies by launch epoch, as shown by Fig. 6-g; the STORM spacecraft design carried enough propellant to allow SOI to be performed on any of the launch epochs shown. This feature of the orbit design gave the mission additional design flexibility as well; in case mass margins needed to be recovered in other parts of the spacecraft design at later stages, this trajectory design allowed the flexibility in choosing launch epochs with a lower ΔV_{SOI}. As a final remark on the Tisserand constant, Fig. 7 shows the computed value for T for the resulting transfer solutions over all 48-days. We can see that T tends to vary between 0.45 and 0.7, and therefore our initial assumption of $T_{\mathrm{ref}} = 0.66$ is near the upper end of this range. Future improvements to the methodology in this paper may include a better way to approximate or predict the required value of T_{ref} for a given launch epoch, and therefore improve the chance that the differential corrector can converge to a solution over a smaller set of grid search parameters.

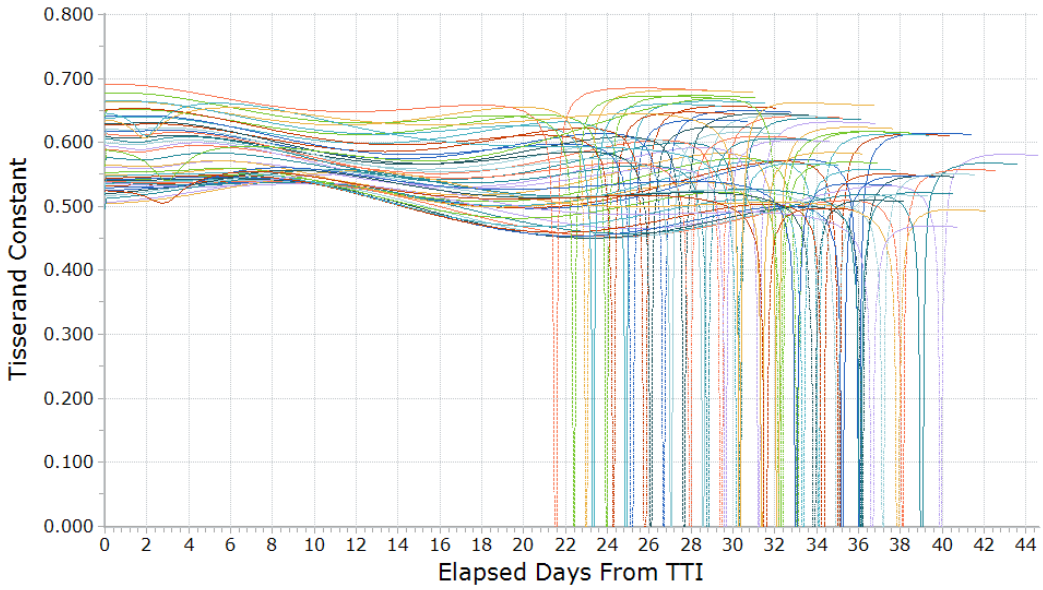

Figure 7. Tisserand constant for resulting transfer solutions for each day during the 48-day period beginning from the LRD.

LIDOV-KOZAI EFFECT (LKE)

Reference 14 gives a detailed historical perspective of the LKE, and the more recent adaptations of the theory. As is often the case with interesting scientific discoveries, the effect was described independently by two people around the same time, and the two are usually both given credit. However, it is also not unusual to find references in the literature calling it the Lidov effect or the Kozai effect. Lidov first published his results in 1961 in Russian,[15] with later translations in English,[16,17] while studying Earth-orbiting artificial satellites under luni-solar perturbations. Kozai examined the problem in 1962 of a heliocentric asteroid being perturbed by Jupiter.[18] The LKE has also received new attention from astronomers for its application to studying exoplanet systems (*e.g.*,

see Reference 14 and references therein). One early application of the LKE was understanding the relatively short time scales before high-eccentricity satellites (*e.g.*, Luna-3 in 1960) reentered the Earth's atmosphere due to third-body perturbations. The LKE was also recently studied on the MMS mission being operated at GSFC, to understand the long-term orbit evolution and the effect of apogee and perigee raising maneuvers on the mission lifetime.[19] The end-of-mission disposal options for the highly-eccentric XMM-Newton mission were studied within the context of the LKE as well.[20]

The orbital stability of STORM's science orbit is heavily influenced by 3rd body perturbations from the Sun and Moon, owing to the large radius. The same perturbations that drive the LKE in highly eccentric orbits will affect STORMs nearly-circular initial science orbit as well, and rapidly drive the science orbit from a circular to a highly eccentric orbit. The LKE was used to plan for STORM's end-of-mission (EOM) disposal plan, which called for the spacecraft to enter the atmosphere within 25 years from EOM to conform to NASA-STD-8719.14.[21] Once STORM's 30-R_E circular orbit evolves into a more eccentric orbit, the secular eccentricity growth happens quickly; the design reference mission had a nominal atmospheric disposal around 9 years after EOM. Figure 8 is a plot of the EOM trajectory, showing the eccentricity growth leading to reentry. The major benefit of this approach is that it leverages orbital dynamics rather than performing a dedicated deorbit maneuver, as a result: (1) additional ΔV for a reentry or graveyard transfer is not needed, and (2) the spacecraft's thruster lifetime did not need to be rated to perform maneuvers at the end of the nominal science mission duration.

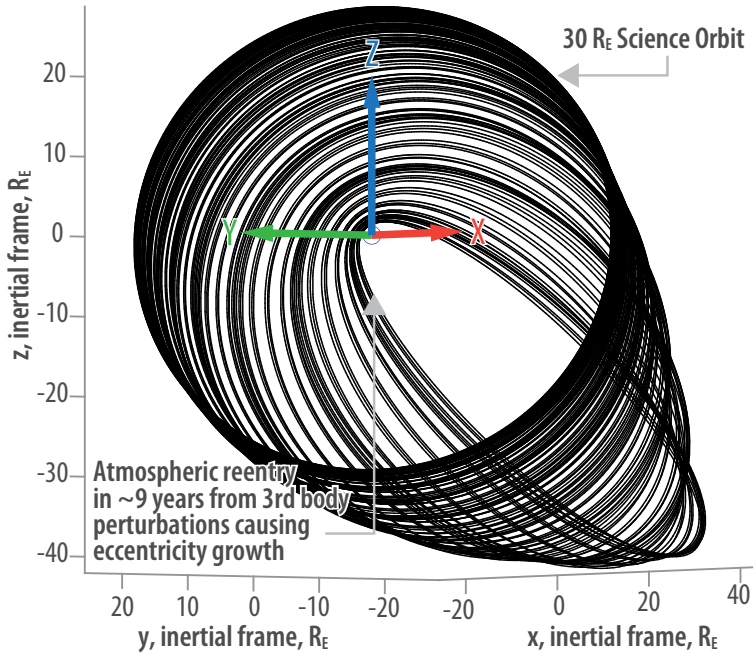

Figure 8. Plot of STORM's end-of-mission disposal trajectory, using the LKE's secular eccentricity growth to reenter in the atmosphere within 9 years without the need for a deorbit maneuver.

From the LKE, we know that the eccentricity will grow for our high-inclination orbit. However, we need to consider the *rate* at which our eccentricity grows, because if we can slow down the eccentricity growth, then we can maximize the length of time that STORM's science orbit requirements (*i.e.*, radius of 30 ± 1 R_E) are met. In addition, if we neglect to carefully examine the LKE, then we may inadvertently select an initial science orbit that fails to meet requirements for the nominal 2-year mission. In Lidov's[17] and Kozai's[18] initial work they both performed a double averaging of the third-body perturbations, over both the short spacecraft period and with respect to the distant perturbing body (either the Sun or the Moon). The result of this double averaging is that three constants of the motion can be identified:[14,17,22] the semimajor axis ($C_0 = a$), the z-component of the angular momentum squared (C_1),

$$C_1 = (1 - e^2)\cos^2 i \tag{4}$$

and the Lidov-Kozai Hamiltonian (C_2),

$$C_2 = e^2 \left(\frac{2}{5} - \sin^2 i \sin^2 \omega \right) \tag{5}$$

where ω is argument of perigee. Broucke[22] leveraged symmetry in the CR3BP and showed that C_2 can be expressed as a function of e, ω, and C_1 as

$$C_2 = e^2\{0.4 - \left[1 - C_1/(1 - e^2)\right] \sin^2 \omega\} \tag{6}$$

and also as a function of equinoctial elements $h = e \sin \omega$ and $k = e \cos \omega$ with

$$C_2 = 0.4(h^2 + k^2) - \left[1 - C_1/(1 - h^2 - k^2)\right] h^2 \tag{7}$$

If we consider a 90-deg ecliptic inclination for STORM, then $C_1 = 0$. Figure 9 shows contour plots generated using Eqs. 6 and 7, where $C_1 = 0$, from which we can now leverage the following understanding. Our desired science orbit will have initial conditions (e, ω) that place us on a C_2 contour. In our case of designing the target science orbit for a given SOI epoch, we are constrained to achieving a near-zero value of e, recognizing that it will have some small initial deviation determined by the targeting tolerances. Our main design variable for designing an optimal science orbit is the initial ω. As seen in Fig. 9, a contour that is closer to the hyperbolic asymptotes will have more rapid eccentricity growth. For a fixed initial value of e, we have the freedom to vary the initial ω to place us on a contour that is further away from the asymptotes and therefore restrict the rate of eccentricity growth.

Ultimately, we are interested in validating the STORM science orbit design in a full ephemeris model (with non-spherical Earth, point-mass Sun and Moon, and SRP described above in the numerical propagation settings), vs. the simplified CR3BP considering only one 3rd-body perturber. Also, the present design does not directly use the phase plots in Fig. 9 because our current tool sets are incapable of converting between oscullating and the Lidov-Kozai double-averaged element set. Therefore, we designed a science orbit optimization scheme as follows: for a candidate initial science orbit (determined by the targeting at SOI for a given epoch), we vary the initial ω at the time of SOI, *i.e.*, $\omega(t_{\mathrm{SOI}})$, and propagate forward, using the full-force ephemeris model, for a fixed amount of time over which to perform the optimization, Δt_{OPT}. The value of $\omega(t_{\mathrm{SOI}})$ that minimizes the future value of $e(t_{\mathrm{SOI}} + \Delta t_{\mathrm{OPT}})$ is selected as the optimal science orbit design.

Given the post-SOI science orbit state that is achieved with the transfer trajectory targeter described in Fig. 4, we then use the science orbit optimizer as follows. Rather than varying the initial

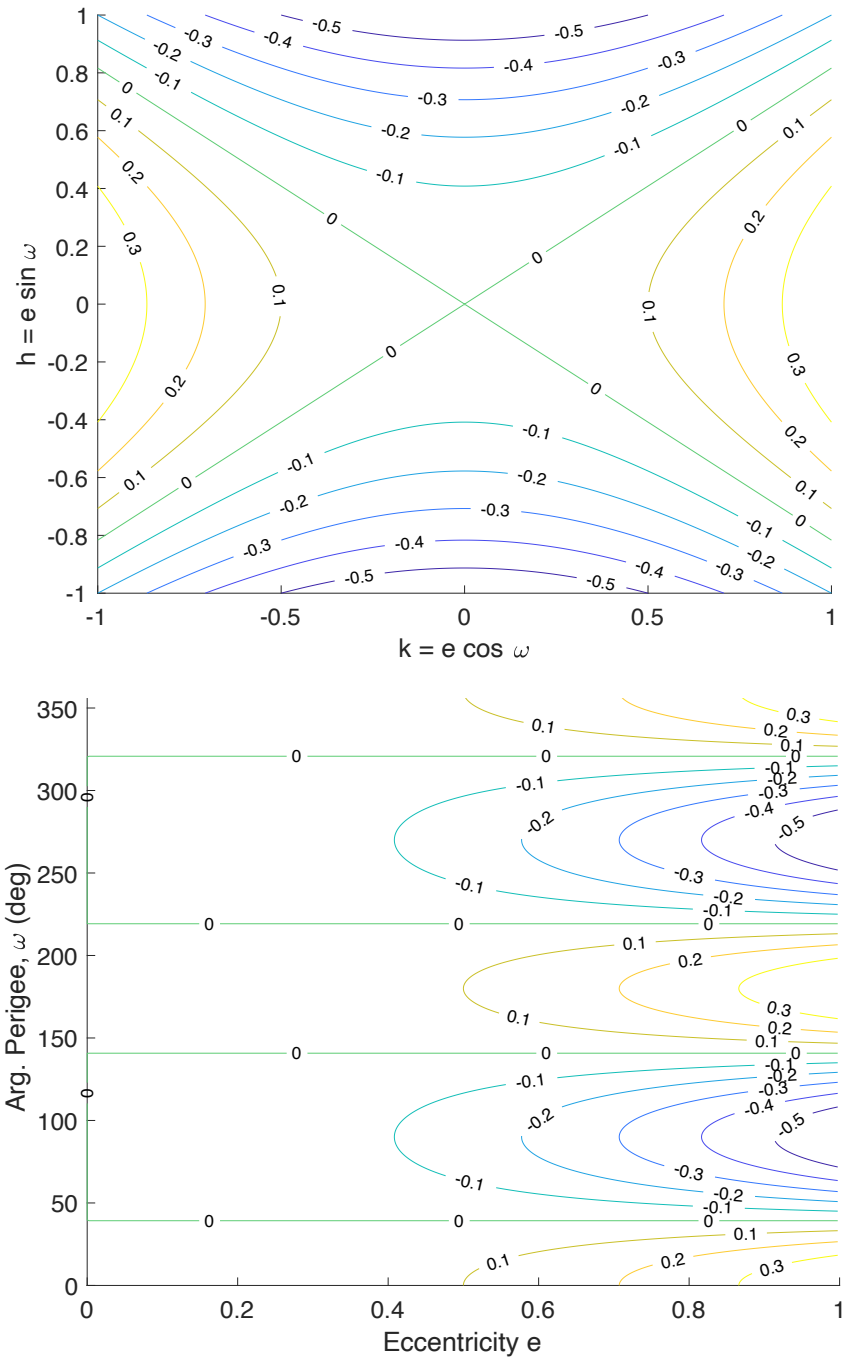

Figure 9. Phase plot showing C_2 countours vs. equinoctial elements k and h (top) and vs. Keplerian elements e and ω (bottom), both for $C_1 = 0$.

science orbit ω directly, we instead propagate to varying test locations post-SOI and insert a small (< 10 m/s) impulsive ΔV to raise or lower the orbit, which gives the effect of setting a new perigee location at that position. Figure 10 shows a plot of $e(t_{\mathrm{SOI}} + \Delta t_{\mathrm{OPT}})$ for $\Delta t_{\mathrm{OPT}} = 4$ years, where the horizontal axis shows the argument of perigee parameterized using these test positions as days after t_{SOI}. It can be seen in Fig. 10 that the eccentricity growth after 4 years can vary greatly, be-

tween less than 0.1 to over 0.8, depending on the location of the initial perigee. The trend line in Figure 10, which has points every 0.5 days, shows that the optimal argument of perigee location occurs at 1 day elapsed time from t_{SOI} (for this particular launch epoch). Because the newly optimized science orbit has radius of apogee and perigee within the tolerances of the initial targeting run, this process can be iterated until the full end-to-end mission completely closes.

In general, it can be risky to use oscullating orbital elements (*i.e.*, compared with mean elements) for this sort of orbit targeting. However, because we are using a fairly large value of $\Delta t_{\mathrm{OPT}} = 4$ years, we are more likely to capture the overall trends in eccentricity growth as opposed to a case where the future value of e happens to land on a peak or trough in the oscullating element trend line. Therefore, we content ourselves with the fact that this approach allows us to find a suitable science orbit that meets mission requirements, without worrying if it is a truly global optimum. Figure 11 shows a plot of the science orbit radius vs. time, with the effect of eccentricity growth clearly visible. The black line shows the result of the above-described science orbit optimization scheme, where the desired science orbit has been achieved with the post-SOI TCM-4 maneuver. This black time series stays within the 30 $\pm$ 1 $\mathrm{R_E}$ radius requirement for nearly 4 years, which is double the science mission lifetime requirement. Conversely, the orange time series shows a slightly perturbed science orbit state, which reflects an example of the resulting orbit if TCM-4 were not performed (*i.e.* if the post-SOI e and ω were slightly off target). We can see that the orange line violates the mission requirements sooner (approximately 2.5 years from SOI), which, although the design meets mission lifetime requirements in this particular case, limits the options for an extended science mission. For comparison, Fig. 12 shows the corresponding plots of ecliptic inclination for this particular case. It is apparent that the ecliptic inclination is not in danger of violating the 90 $\pm$ 10 deg requirement in either nominal or perturbed cases, because it tends to vary periodically instead of growing secularly as was the case with eccentricity.

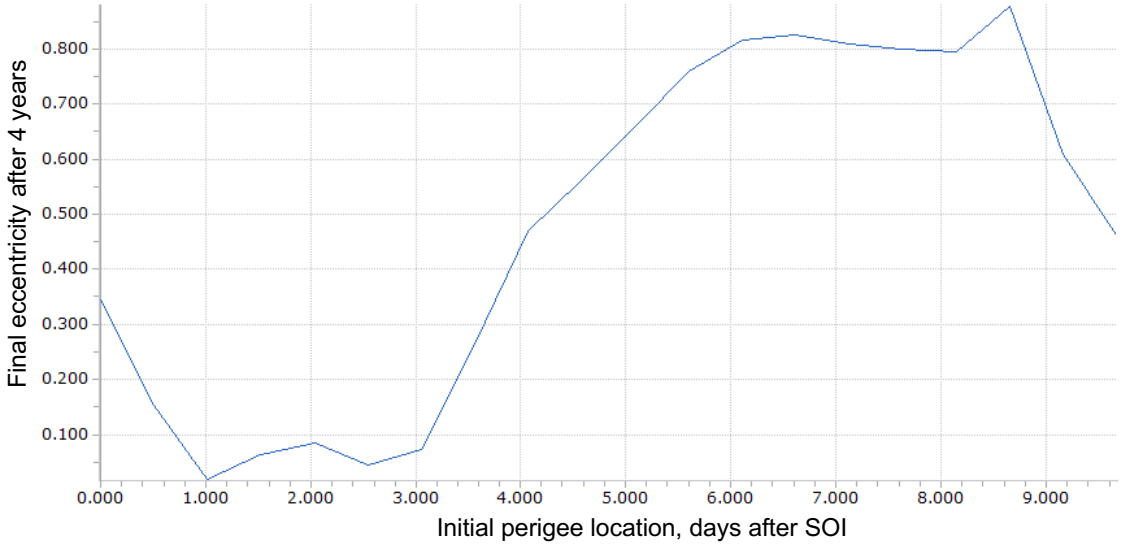

Figure 10. Plot illustrating the science orbit optimization process, where the future eccentricity after 4 years is minimized by setting the location of perigee.

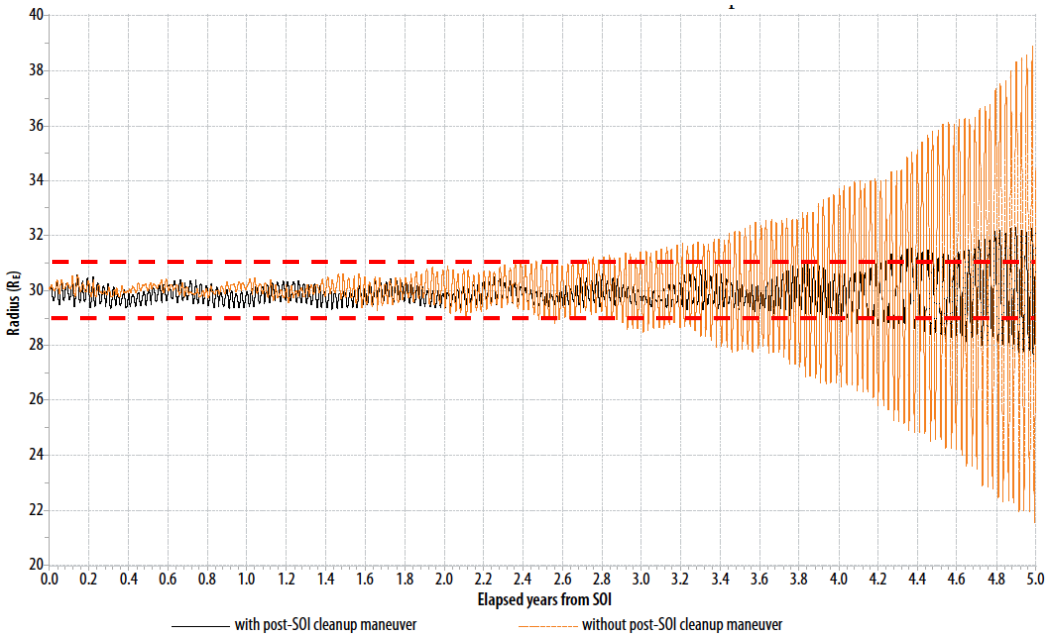

Figure 11. Plot of orbital radius vs. time, with 30 $\pm$ 1 R_E requirement denoted with red dashed lines. The effect of eccentricity growth can be compared between two cases: a non-optimal science orbit (in orange) representing the case where TCM-4 (science orbit clean-up) is not performed, and an optimal case (in black) representing where TCM-4 has been performed.

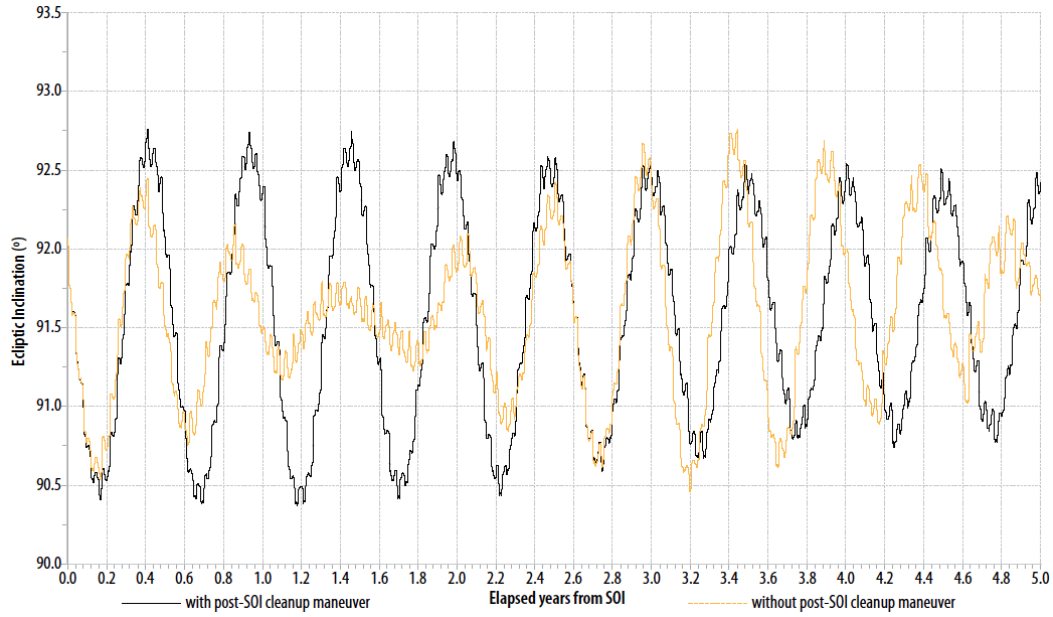

Figure 12. Plot of ecliptic inclination vs. time, showing mostly periodic and non-secular variations: a non-optimal science orbit (in orange) representing the case where TCM-4 (science orbit clean-up) is not performed, and an optimal case (in black) representing where TCM-4 has been performed.

MONTE CARLO ANALYSIS OF SCIENCE ORBIT STABILITY

In addition to examining the stability of the science orbit within the theory of the LKE, we performed Monte Carlo analysis to ensure that the orbit would meet requirements even in the presence of additional forces and uncertainties. A benefit of the STORM mission design is the operational simplicity achieved by not requiring orbit stationkeeping maneuvers after entering the science orbit. Upon completion of TCM-4, no additional orbit maneuvers are required to meet the mission requirements listed above. We can demonstrate through the Monte Carlo analysis that after TCM-4, the mission has nearly 100% probability of meeting the science orbit requirement of 30 ± 1 R_E for the required 2-year mission life, with low sensitivity to orbit dispersions or unmodeled accelerations.

In addition to the numerical propagator settings already mentioned above, our Monte Carlo analysis used several additions to the force model once TCM-4 is completed (Table 1), to determine the effect of small perturbations on our concept-of-operations that eliminates the need for science orbit station-keeping. The position and velocity dispersions post-TCM-4 are informed by the expected navigation error and maneuver execution error. The momentum unloads are modeled by applying an impulsive ΔV at a frequency of once per 44 days, where each unload gets a newly sampled ΔV vector at each occurrence.

Table 1. Force model perturbations used in post-TCM-4 science orbit stability Monte Carlo analysis.

Force	Model	Distribution
SRP Scale Factor	Constant bias	Normal, $\mathcal{N}(\mu = 1, \sigma = 0.05)$ unitless
Momentum Unload ΔV	Impulsive ΔV vector	Normal, $\mathcal{N}(\mu = 0, \sigma = 1)$ mm/s, each component
Unmodeled Acceleration	Polynomial acceleration with 6-hour batches	Normal, $\mathcal{N}(\mu = 0, \sigma = 3 \times 10^{-12})$ km/s^2, each component, per batch

The Monte Carlo analysis used 1000 trials, each of which were propagated until the 30 +/- 1 R_E radius requirement was violated, and the time was recorded. Figure 13 shows the resulting histogram with a probability normalization. Note that although the bins in the distribution appear sparse, this figure accurately reflects all 1000 samples. The distribution shows several peaks centered on certain times between 4 and 4.3 years. The explanation for these peaks becomes clear after examining Figure 14, which shows the time-history of the radius for a selection of the first 50 samples. The peaks in the probability distribution show when a given sample first intersects the 30 +/- 1 R_E boundaries indicated in Fig. 14. It is clear from Fig. 13 that all 1000 samples meet science orbit requirements for at least 4 years, and there is nearly 100% probability that requirements will be met for 2 years as required by the mission. Figs.13 and 14 illustrate that the science orbit stability is not significantly affected by the expected dispersions and perturbations once TCM-4 is completed.

MONTE CARLO ANALSIS OF END-OF-MISSION

Additional Monte Carlo analyses were performed to assess the likelihood that STORM would reenter as required, regardless of the epoch or luni-solar geometry at the beginning of EOM. In other words, although the transfer trajectory design focused on a 48-day window of launch opportunities beginning with the LRD, and the corresponding nominal 2-year mission, this Monte Carlo analysis ensures that the LKE-based approach to reentry disposal was robust to a wide variation in epochs and geometries. During the science mission phase, the spacecraft orbital parameters are free to drift due to natural perturbations without any additional maneuvers. The initial orbit conditions (at EOM epoch) are a result of these natural drifts in orbital conditions, and are given in Table 2.

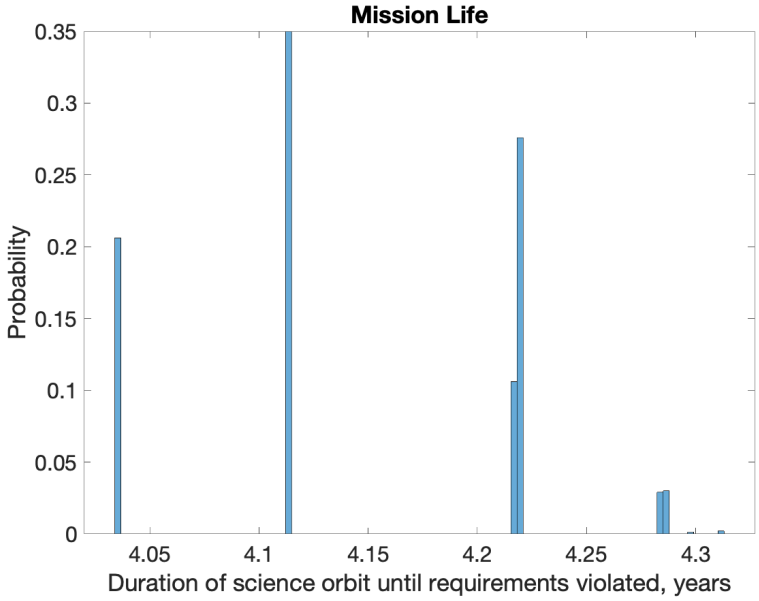

Figure 13. Histogram of science orbit Monte Carlo stability results, showing that the science orbit duration meets the radius requirement of 30 $\pm$ 1 R_E for the required 2-year lifetime for all 1000 samples.

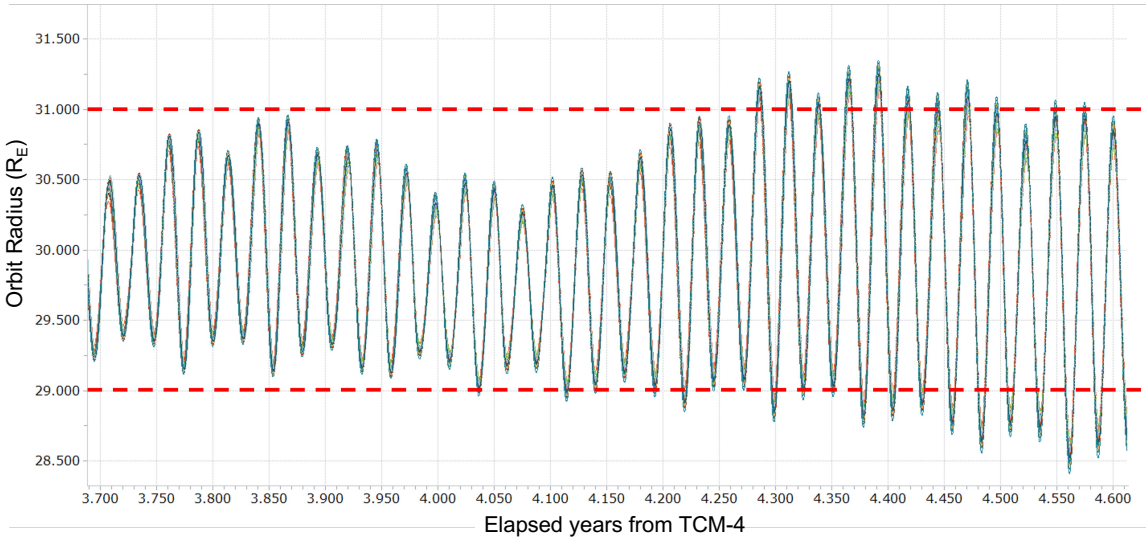

Figure 14. Radius vs. time for the first 50 Monte Carlo samples, showing how peaks in the probability distribution relate to the science orbit requirement of 30 $\pm$ 1 R_E.

The distributions on EOM conditions represent the total set of all possible initial conditions to examine when assessing reentry, regardless of launch opportunity or transfer orbit geometry. The distributions on radius of apogee, radius of perigee, and ecliptic inclination represent a reasonable set of orbits that have met science orbit requirements (i.e. radius of 30 +/- 1 R_E, ecliptic inclination of 90 +/- 10 deg) over the mission lifetime. The year-long sampling of EOM epochs ensures that

a thorough sweep of possible lunar and solar positions (and resulting perturbations) are sampled, since luni-solar perturbations are the driving factor in STORM's eccentricity growth and eventual reentry caused by the LKE. The Monte Carlo simulation used a sample size of $N = 3000$. Note that the sampled radius of apogee (r_a) and perigee (r_p) are sorted to ensure that $r_a > r_p$.

Table 2. Monte Carlo reentry simulation initial conditions at EOM. Note that the dispersions in radius result from no active control over the 2-year mission, and are approximately 3 orders of magnitude larger than the expected dispersions post-TCM-4.

Parameter	Distribution
EOM epoch (days from LRD + 2 years)	Uniform, $\mathcal{U}\,[0, 365]$ days
Radius of apogee	Normal, $\mathcal{N}(\mu = 30, \sigma = 0.3)$ R_E
Radius of perigee	Normal, $\mathcal{N}(\mu = 30, \sigma = 0.3)$ R_E
Ecliptic inclination	Normal, $\mathcal{N}(\mu = 90, \sigma = 3.3)$ deg
Right ascension of ascending node	Uniform, $\mathcal{U}\,[0, 365]$ deg
Argument of perigee	Uniform, $\mathcal{U}\,[0, 365]$ deg
True anomaly	Uniform, $\mathcal{U}\,[0, 365]$ deg

In contrast to most Earth-orbiting spacecraft with an option to perform an atmospheric disposal, the details of the atmospheric density model has negligible impact on STORM's reentry lifetime calculation, because the spacecraft only spends a few revolutions in its highly eccentric orbit with perigee below ≈700 km altitude before reentry. The spacecraft is propagated until its radius reaches 200 km altitude, after which propagation is halted and the reentry lifetime (i.e. time from EOM to reentry) and final orbit state are recorded.

Figure 15 shows a normalized histogram of the resulting lifetimes from the Monte Carlo samples. In most cases, STORM will reenter well before the 25-year requirement; summing the bins having

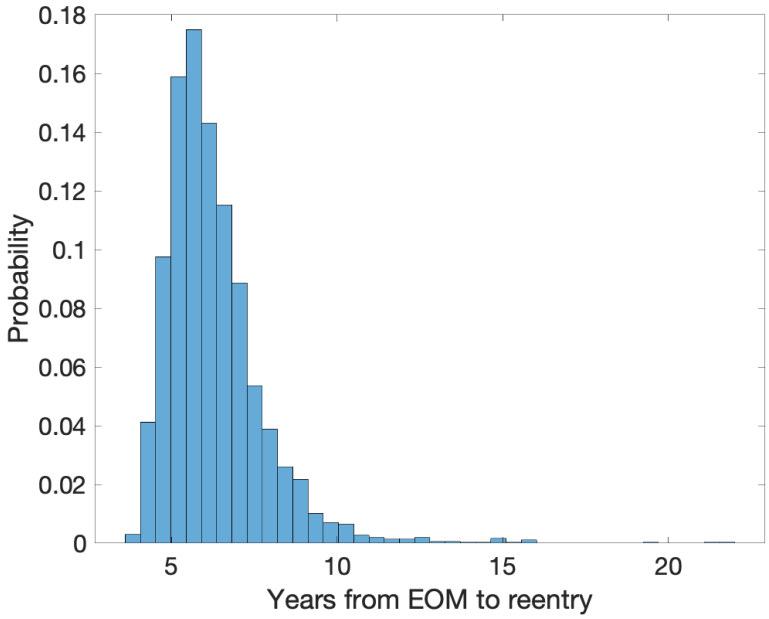

Figure 15. Reentry lifetime histogram results from Monte Carlo simulation, showing that 100% of the $N = 3000$ samples reenter within the 25-year requirement.

a lifetime of 9 years or less shows that there is approximately 94% probability of the spacecraft reentering within 9 years from EOM. Likewise, Figure 15 shows that over 99% of samples reenter within 15 years, and 100% of samples reenter within 22 years from EOM.

CONCLUSIONS

The STORM mission's Phase A design leveraged Tisserand's criterion to improve the efficiency of a grid search for transfer trajectory solutions in a ephemeris model differential corrector, enabling a high-eccentricity out-bound transfer leading to an in-bound lunar gravity assist to achieve the required inclination change into the target science orbit. Although not optimized for minimum fuel usage, the presently described approach found launch solutions on each day out of a 48-day period, including nearly two full lunar orbital periods, enabling a robust and flexible mission design. The design of the science orbit leveraged the predictions of the Lidov-Kozai effect, to ensure that eccentricity growth can be minimized during the operational 2-year science mission, yet still enabling the spacecraft to naturally reenter within the 25-year disposal requirement. The science orbit's secular eccentricity growth was minimized using a numerical procedure in an ephemeris model that selected the argument of perigee that minimized eccentricity after 4 years. Monte Carlo analysis verified that the science orbit design had the necessary stability to meet requirements over the operational mission and for end-of-mission disposal. The numerical simulations showed that 100% of samples met the mission's eccentricity requirements for the 2-year science mission, and that around 99% of samples would reenter the atmosphere within 15 years.

ACKNOWLEDGMENT

We thank Conrad Schiff of NASA GSFC for graciously performing a peer review of this manuscript, and for many useful suggestions during the STORM design study.

REFERENCES

[1] B. M. Walsh, M. R. Collier, E. Atz, L. Billingsley, J. M. Broll, H. K. Connor, D. Chornay, T. Cragwell, N. Dobson, S. Eckert, D. Einhorn, G. Gallant, K. Jackson, S. Karki, J. Kujawski, K. D. Kuntz, V. Naldoza, R. A. Nutter, J. Moore, C. O'Brien, A. Perez-Rosado, F. S. Porter, D. G. Sibeck, K. Simms, W. Skelton, N. Thomas, D. L. Turner, A. Yousuff, A. Weatherwax, A. Zosuls, and E. Thomas, "The Cusp Plasma Imaging Detector (CuPID) CubeSat Observatory: Mission Overview," *Journal of Geophysical Research (Space Physics)*, Vol. 126, Apr. 2021, p. e29015, 10.1029/2020JA029015.

[2] B. Walsh, M. Collier, K. Kuntz, F. Porter, D. Sibeck, S. Busk, H. Connor, M. Galeazzi, V. Naldoza, S. Sembay, N. Thomas, and R. Nutter, "Heliospheric imaging and science from the Moon with LEXI," *AGU Fall Meeting Abstracts*, Vol. 2021, Dec. 2021, pp. SH23A–06.

[3] C. Circi, F. Grazini, and P. Teofilatto, "Moon Assisted Out of Plane Maneuvers of Earth Spacecraft," *Journal of the Astronautical Sciences*, Vol. 49, 2001, pp. 363–383.

[4] C. A. Ocampo, "Transfers to Earth centered orbits via lunar gravity assist," *Acta Astronautica*, Vol. 52, No. 2-6, 2003, pp. 173–179.

[5] R. Ramanan and V. Adimurthy, "Precise lunar gravity assist transfers to geostationary orbits," *Journal of guidance, control, and dynamics*, Vol. 29, No. 2, 2006, pp. 500–502.

[6] S. Choi, J. Carrico, M. Loucks, H. Lee, and S. Kwon, "Geostationary Orbit Transfer with Lunar Gravity Assist from Non-equatorial Launch Site," *Journal of the Astronautical Sciences*, Vol. 68, 2021, pp. 1014–1033.

[7] J. Betts, "Optimal Lunar Swingby Trajectories," *Journal of the Astronautical Sciences*, Vol. 55, No. 3, 2007, pp. 349–371.

[8] T. Lee, D. Dunham, S. Hsu, C. Roberts, and C. Engel, "Large inclination change using lunar-swingby techniques," *AIAA/AAS Astrodynamics Conference, Minneapolis, MN*, 1988, p. 4290. AIAA 88-4290.

[9] W. McLaughlin and S. Miller, "The Shadow Effect and the Case of Félix Tisserand: The most eminent astronomer who never came to popular attention was lost in the shadow of his countryman, Pierre-Simon Laplace," *American Scientist*, Vol. 92, No. 3, 2004, pp. 262–267.

[10] A. E. Roy, *Orbital Motion, Fourth Edition*, ch. 5, pp. 121–122. New York: Taylor and Francis Group, 2005.

[11] N. Strange and J. Longuski, "Graphical Method for Gravity Assist Trajectory Design," *Journal of Spacecraft and Rockets*, Vol. 39, No. 2, 2002, pp. 9–16.

[12] K. Hughes, P. Edelman, S. Saikia, J. Longuski, M. Loucks, J. C. Jr., and D. Tito, "Fast Free Returns to Mars and Venus with Applications to Inspiration Mars," *Journal of Spacecraft and Rockets*, Vol. 52, No. 6, 2015, pp. 1712–1735.

[13] S. Campagnola and R. Russell, "Endgame Problem Part 2: Multibody Technique and the Tisserand-Poincaré Graph," *Journal of Guidance, Control, and Dynamics*, Vol. 33, No. 2, 2010, pp. 476–486.

[14] I. Shevchenko, *The Lidov-Kozai Effect – Applications in Exoplanet Research and Dynamical Astronomy*, ch. 1, pp. 1–9. Astrophysics and Space Science Library, Switzerland: Springer International Publishing, 2017.

[15] M. Lidov, "Evolution of artificial planetary satellites under the action of gravitational perturbations due to external bodies," *Iskusstviennye Sputniki Zemli (Artificial Satellites of the Earth)*, Vol. 8, 1961, pp. 5–45. (in Russian).

[16] M. Lidov, "The evolution of orbits of artificial satellites of planets under the action of gravitational perturbations of external bodies," *Planetary and Space Science*, Vol. 9, No. 10, 1962, pp. 719–759.

[17] M. Lidov, "Evolution of the Orbits of Artificial Satellites of Planets as Affected by Gravitational Perturbation from External Bodies," *AIAA Journal*, Vol. 1, No. 8, 1963, pp. 1985–2002.

[18] Y. Kozai, "Secular Perturbations of Asteroids with High Inclination and Eccentricity," *The Astronomical Journal*, Vol. 67, No. 9, 1962, pp. 591–598.

[19] T. Williams, E. Palmer, J. Hollister, D. Godine, N. Ottenstein, and R. Burns, "Lunisolar Perturbations of High-Eccentricity Orbits Such as the Magnetospheric Multiscale Mission," *AAS/AIAA Astrodynamics Specialist Conference, Portland, ME*, 2019. AAS 19-914.

[20] C. Colombo, "Long-Term Evolution of Highly-Elliptical Orbits: Luni-Solar Perturbation Effects for Stability and Re-entry," *AAS/AIAA Space Flight Mechanics Meeting, Williamsburg, VA*, 2015. AAS 15-395.

[21] National Aeronautics and Space Administration, "Process for Limiting Orbital Debris," April 2019. NASA-STD-8719.14B.

[22] R. Broucke, "Long-Term Third-Body Effects via Double Averaging," *Journal of Guidance, Control, and Dynamics*, Vol. 26, No. 1, 2003, pp. 27–32.